NASA Technical Memorandum 100877

Characterization of Fatigue Crack Initiation and Propagation in Ti-6Al-4V With Electrical Potential Drop Technique

Sreeramesh Kalluri
Sverdrup Technology, Inc.
NASA Lewis Research Center Group
Cleveland, Ohio

and

Jack Telesman
National Aeronautics and Space Administration
Lewis Research Center
Cleveland, Ohio

July 1988

NASA

CHARACTERIZATION OF FATIGUE CRACK INITIATION AND PROPAGATION IN Ti-6Al-4V WITH ELECTRICAL POTENTIAL DROP TECHNIQUE

Sreeramesh Kalluri
Sverdrup Technology, Inc.
NASA Lewis Research Center Group
Cleveland, Ohio 44135

and

Jack Telesman
National Aeronautics and Space Administration
Lewis Research Center
Cleveland, Ohio 44135

ABSTRACT

Electrical potential methods have been used in the past primarily to monitor crack length in long-crack specimens subjected to fatigue loading. In this study an attempt was made to develop test procedures for monitoring the fatigue crack initiation and the growth of short fatigue cracks in a turbine disk alloy with the electrical potential drop technique (EPDT). In addition, the EPDT was also applied to monitor the fatigue crack growth in long-crack specimens of the same alloy. The experimental program was conducted as part of an AGARD-sponsored roundrobin program on titanium alloy engine disk material. The resolution of the EPDT for different specimen geometries was determined. Factors influencing the EPDT are identified and the applicability of EPDT in implementing damage-tolerant design concepts for turbine disk materials is discussed. The experimental procedure adopted and the results obtained are presented. No substantial differences were observed between the fatigue crack growth data of short- and long-crack specimens.

INTRODUCTION

During the last 10 years the electrical potential drop technique (EPDT) has gained a substantial level of acceptance as a tool to measure fatigue crack growth (FCG) rates of long-crack specimens. This technique is based on the changing direct-current potential as a function of crack length (refs. 1 to 5). The two main advantages of the EPDT over optical surface measurements are (1) the technique lends itself to full automation and (2) the crack length data measured by the EPDT reflect the average crack profile through the entire thickness of the specimen whereas the optical crack length measurement technique measures only the intersection of the crack front with the specimen surface.

The use of the EPDT has been almost exclusively limited to FCG testing of long-crack specimens. However, other fatigue research areas might benefit from the use of this technique, if proper methodology for its application can be identified. The areas of research that could benefit from the application of the EPDT are as follows: (1) fatigue crack growth of short cracks, (2) crack initiation under low cycle fatigue, and (3) measurement of damage under creep

at elevated temperatures. The question arises as to whether the EPDT is sensitive enough to be used in these applications. If the answer to this question is affirmative, then development of procedures for optimizing data generation with EPDT is needed.

The need to understand FCG of short cracks as well as early crack detection under low cycle fatigue (LCF) is driven by recent efforts to implement the damage-tolerant design concept for turbine engine components. The damage tolerance philosophy is based on the assumption that crack-like defects exist at every critical location and that the growth of these defects under actual operating conditions can be predicted. Inspection at regular intervals will screen out the components that have insufficient remaining life. The inspection interval is a function of the maximum allowable crack size, the minimum reliably detectable crack size, and the available crack growth data base. Since most of the critical engine components are subjected to high stresses, only very small cracks can be tolerated before the fracture toughness of the material is reached. Thus, understanding of crack initiation and the early stages of crack growth is needed before damage tolerance methodology can be fully implemented. At present, application of this methodology is hindered by the inability to reliably predict the FCG behavior of short cracks. Research on short-crack behavior as well as on crack initiation is considerably hindered by labor-intensive data collection methods, such as replication. A successful application of the easily automatable EPDT to study both crack initiation and short-crack growth behavior would provide a substantial impetus to the implementation of the damage tolerance methodology for the design of engine components.

A test program was conducted to determine the feasibility of using EPDT to study crack initiation and short-crack growth behavior of Ti-6Al-4V turbine disk forgings. This program was conducted as part of a cooperative roundrobin program sponsored by AGARD (refs. 6 to 8).

EXPERIMENTAL PROCEDURE AND RESULTS

The material properties of the Ti-6Al-4V alloy turbine disk forging used in this study are shown in table I. A representative micrograph of the alloy is shown in figure 1. The microstructure consists of equiaxed α grains (light) in a transformed β matrix (dark) containing coarse acicular α. The average size of the α grains is approximately 25 μm.

The test program consisted of four types of experiments, each using a different specimen machined from the turbine disk forging. The geometry of each of the four types of specimens is illustrated in figure 2. The specimens were supplied by Rolls Royce Ltd. Low-cycle fatigue and crack initiation data were generated by using smooth cylindrical and flat double-edge-notched specimens, respectively. FCG data in the short and long crack regimes were obtained by using corner crack specimens and ASTM compact tension specimens, respectively. The test matrix used in the program is shown in table II. The EPDT was used to monitor crack initiation and propagation for all types of testing with the exception of low-cycle fatigue experiments, which were conducted to obtain baseline fatigue life data.

All the experiments were conducted at room temperature in the ambient environment on servohydraulic fatigue testing machines. A trapezoidal load

waveform with R = (minimum load/maximum load) = 0.1 was used in each of the experiments. A schematic illustration of the load waveform is shown in figure 3. The frequency of the load waveform was 0.25 Hz unless indicated otherwise. The experimental procedure and the results of each type of test are presented in the following sections.

Low-Cycle Fatigue Experiments

Smooth cylindrical specimens (fig. 2(a)) were used to conduct the LCF experiments. No attempt was made to monitor crack initiation or propagation in these experiments. Prior to testing, the bending strains of the test rig were measured to be less than 2 percent. Tests were conducted under load control. Axial strain was monitored with a 12.7-mm-gage-length extensometer. Stress-strain hysteresis loops as well as load and strain versus time data were recorded throughout each LCF test on X-Y recorders and strip charts, respectively. Tensile strain ratchetting was observed in all of the experiments. The LCF data are tabulated in table III and plotted in figure 4. The solid line represents the least-squares fit to the data points.

Crack Initiation Experiments

Flat double-edge-notched specimens (fig. 2(b)) with a nominal stress concentration factor K_t of 2.2 were used in these experiments. The deviation from the loading axiality was measured under elastic conditions to be 3.7 percent, which was less than maximum allowable value of 5 percent (ref. 7) and hence was considered acceptable. EPDT was used to establish crack initiation. One set of potential probes (0.5-mm-diameter titanium wire) was welded diagonally at opposite corners of each notch. The reference voltage was generated by welding titanium wire reference leads across the notch of an identical double-edge-notched specimen made of Ti-6Al-4V alloy. This procedure ensured that the reference voltage signal was approximately equal to the notch voltage signal. The instrumented double-edge-notched specimen is shown in figure 5. The electrical current was supplied to the specimen by a constant dc current source.

The reference voltage V_{ref} and the notch voltages V_{n1} and V_{n2} were recorded throughout each test on strip chart recorders. Crack initiation life was defined in the AGARD roundrobin (ref. 7) as the number of cycles $N_{1\%}$ at which the normalized notch voltage V_n/V_{ref} was 1 percent above the initial value. The normalized notch voltage versus number of cycles was plotted for the notch that exhibited a more rapid increase in the voltage with cycles. A typical normalized voltage versus cycles plot is depicted in figure 6. It is evident from this figure that fatigue damage had actually started well before the normalized notch voltage increased by 1 percent. The experimental data generated by using the double-edge-notched specimens are tabulated in table IV. The dashed and solid lines in figure 7 represent least-squares fits to the crack initiation and failure data, respectively. The crack initiation life determined by the EPDT for the 1 percent normalized voltage increase criterion was typically about 92 percent of the failure life of the double-edge-notched specimen.

Fatigue Crack Growth of Short Cracks

The fatigue crack growth behavior of short cracks was investigated with corner crack specimens (fig. 2(c)). The crack growth was monitored both by an optical traveling microscope and EPDT. Electrical potential across the corner crack was calibrated by using surface crack length a_s measured with the traveling optical microscope.

Two electrical titanium wire probes (0.05-mm diameter) were spot welded on either side of the corner crack. The details of an instrumented corner crack specimen are shown in figure 8. Because of the strong influence of the location of probes on the calibration, caution was taken in locating the probes right on the edges of the corner notch. The influence of the distance between the electrical probes on the crack length calibration is illustrated in figure 9 (from ref. 7). The reference voltage was provided by welding a separate set of electrical probes on another corner crack specimen. A dc current of 10 A was supplied in series to the reference specimen as well as to the FCG corner crack specimen. A fatigue crack was initiated in the corner crack specimen at a frequency of 5 Hz. The actual crack propagation test was conducted at 0.25 Hz using the waveform shown in figure 3. The stress intensity factor was calculated by the formula shown in appendix A.

The crack length at the specimen surface a_s was monitored throughout the experiment with the optical traveling microscope. Both the corner crack voltage V_c and the reference voltage were recorded throughout the experiment on strip chart recorders. The final average crack length was obtained by averaging five radial measurements taken at 0°, 22.5°, 45°, 67.5°, and 90° from the crack corner. The average calculated crack length a was 1.078 times a_s. A master calibration curve was first generated for the corner crack specimens by plotting the optically measured surface crack length a_s against the parameter $V_c/V_{ref}w$ at several different crack lengths, where w is the width of the specimen. The master calibration curve for the corner crack specimens is shown in figure 10. In subsequent corner crack growth experiments the master calibration curve was used to normalize the obtained test data. This normalization was necessary to account for small variations in the distance between the electrical probes of the corner crack specimens. The FCG data obtained through this procedure as well as the equation fitting the data are shown in figure 11.

Representative fractographs of a corner crack specimen at the early and intermediate stages of the FCG curve are shown in figure 12. In the low ΔK (stress intensity range) region, when the crack was short, the failure had a crystallographic appearance (fig. 12(a)). In the intermediate ΔK region the failure occurred mostly through a striation-forming process (fig. 12(b)).

Fatigue Crack Growth of Long Cracks

Fatigue crack growth investigation of long cracks was performed with compact tension (CT) specimens (fig. 2(d)). In order to provide current input to the specimen, two holes were drilled and tapped on the top and bottom surfaces of the specimen (fig. 13). Two electrical potential probes (0.5-mm-diameter titanium wire) were welded to the notch edge at diagonally opposite corners as indicated in figure 13. An identical compact tension specimen also made of Ti-6Al-4V alloy was used to provide the reference voltage. Direct electric current was supplied to the CT specimen and the reference specimen in series.

All the CT specimens were precracked at a frequency of 5 Hz. The crack propagation, however, was conducted at 0.25 Hz by using the trapezoidal waveform shown in figure 3. The stress intensity factor for the CT specimens was calculated per ASTM E647 (ref. 9).

The notch and reference potential values were recorded throughout the experiment on strip chart recorders. The crack was propagated under cyclic loading until a/w was approximately equal to 0.65. At this stage the specimen was separated into two pieces and the final crack length before fracture was measured optically. The final average crack length was determined by averaging five measurements taken at 0, 25, 50, 75, and 100 percent of the specimen width. The calibration equations used to calculate the crack lengths are shown in appendix B. The da/dN versus ΔK plot for the compact tension specimen is shown in figure 14. The FCG data appear to fall into two regimes. As a result, two equations were used to fit the data.

DISCUSSION

The driving force behind this work is the need for a test methodology to be used in conjunction with the implementation of damage-tolerant design concepts for turbine engine components. In particular, screening tests are required for studying crack initiation and short-crack propagation in the candidate materials. These particular requirements make it imperative that the testing methodology have sufficient resolution for the detection and study of small flaws.

Resolution

Resolution is defined as the smallest increment in the crack length that can be accurately measured with a given crack length measurement technique. The results of this work show that the resolution of the EPDT depends on the following parameters: (1) the magnitude of the dc current used, (2) the geometry of the specimen, and (3) the distance between the electrical potential probes. In general the resolution of the EPDT increases with an increase in the dc current. However, large dc currents can also induce undesirable specimen heating. This phenomenon limits the extent to which the dc current can be increased and hence the resolution. In this program, at a dc current of 10 A, crack length resolutions of 0.025 and 0.020 mm were obtained for the corner crack and compact tension specimens, respectively. The influence of the location of potential probes on the calibration for a corner crack specimen (fig. 9) indicates that resolution of the crack length measurement depends on the distance between the probes.

Besides the location of the leads, other factors can have a substantial effect on the EPDT output. Substantial effects on the crack length resolution were caused by small drifts in the current supplied to the specimens. These small drifts would have no appreciable effect on long-crack specimens, but for the double-edge-notched and corner crack specimens the small drifts result in changes in the output voltage that can mask the crucial initial fatigue damage. The use of a reference specimen completely compensated for the small drifts in the dc current, thus significantly improving the resolution of the system.

Additional Factors Affecting EPDT

Hartman and Johnson (ref. 10) identified three additional factors that can influence the dc electrical potential reading: (1) material resistivity, (2) thermally induced electric potential, and (3) crack closure.

The resistivity of the test specimen material can change as a result of either plastic deformation at the crack tip or a change in the test specimen temperature during the fatigue crack growth test. If large plastic deformations occur at the crack tip, the electrical potential readings could lead to erroneous crack length measurements. However, this problem can be minimized by properly designing the test specimen geometry. Thermally induced resistivity changes in the test specimen can be minimized by carefully controlling the temperature of the testing environment.

In general, the probes used in the potential drop measurements are made of a different material than the test specimen itself. As a result, a thermally induced potential (due to a thermocouple effect) can exist between the electrical potential probes (ref. 10). This thermally induced potential can affect the change in potential arising from the growth of the fatigue crack. However, the thermally induced potential can be minimized by maintaining the junctions of the two different metals at the same temperature (fig. 5(b)).

Fatigue crack closure can also affect the dc potential measured by the probes. During crack closure electrical contact can occur between the two faces of the crack and lower the resistance of the specimen. When the current is constant, lower resistance can reduce the electrical potential measured by the electrical probes. Hence, crack closure can lead to periodic fluctuations in the electrical potential measured by the probes under cyclic loadings. However, electrical potential corresponding to the actual crack length can be obtained by measuring the potential at the peak tensile load, where there is no crack closure (refs. 1 and 10). The effect of crack closure on the measured electric potential has been observed to be more pronounced in vacuum than in air because of the lack of nonconducting oxide layer formation in vacuum (ref. 11).

FCG of Short-Crack Specimens

A corner crack specimen was used to simulate the fatigue behavior that could occur around the turbine disk bolt holes, where the fatigue cracks are short. It has been shown by researchers (e.g., refs. 12 to 14) that cracks short enough in length exhibit accelerated fatigue crack growth rates when compared with long, well developed cracks at equivalent stress intensity. The FCG results obtained in this study with the EPDT, however, do not exhibit the short-crack effect and show no substantial difference from the long-crack data (fig. 15). The most likely explanation for this behavior is that the short-crack effect is usually noticeable when the crack length is either smaller than or equal to the grain size. In this study the initial crack length for the corner crack specimen was 0.25 mm while the grain size was 25 μm. Thus the crack front was embedded in many different grains, and the short-crack behavior was not observed. Gangloff (ref. 3), also using EPDT and specimens containing small initial flaws, could not detect a short-crack growth regime. In this instance again, the initial flaw might have been larger than the grain size.

The corner crack specimen is capable of capturing short-crack effects in a coarse-grained material (ref. 8).

As mentioned earlier, the resolution of the EPDT system was measured to be 0.025 mm for the corner crack specimens. It is possible to accurately measure the early stages of crack growth in corner crack specimens with such a resolution. However, short-crack behavior can be successfully studied in this type of specimen only if the grain size of the alloy is larger than the initial notch. Another set of problems arises in specimens where the cracks initiate naturally, such as the double-edge-notched specimen. One of the problems is that the leads are located further from the crack, thus reducing the system resolution. Another important factor is that for both the notched and smooth specimens a number of different cracks can initiate. The resulting voltage change is then indicative of the cumulative effect of a number of cracks and thus cannot be used to calculate the length of a given crack. However, the EPDT can be used for these types of specimens in conjunction with another technique for measuring crack length, such as replication. For example, EPDT can be used to detect crack initiation and then replication can be used to measure the surface crack length.

Damage Tolerance Approach

The results presented in this report show that EPDT can play a significant role as part of the test methodology needed for implementing damage-tolerant design concepts. In spite of its shortcomings the EPDT has a role as an inexpensive screening test to evaluate the small-defect tolerance of candidate turbine engine materials. Indeed, Van Stone et al. (ref. 4) have used EPDT as such a screening tool in evaluating the damage tolerance of nickel-base superalloys for turbine disk applications. At its present stage the EPDT is not the ultimate methodology for the damage tolerance approach; however, its inexpensive cost as well as its compatibility with other techniques makes it a very useful tool.

CONCLUSIONS

The EPDT technique was successfully applied in determining the fatigue crack initiation and monitoring the fatigue crack growth in two different specimens of Ti-6Al-4V alloy. In this study no substantial differences were observed between the FCG data of corner crack and compact tension specimens.

The resolution of the crack length obtained at a dc current of 10 A was 0.025 mm for a corner crack specimen. For the same magnitude of dc current the crack length resolution observed for a compact tension specimen was 0.020 mm. Even though EPDT is not the ultimate methodology for the damage tolerance approach, it can be used as an inexpensive screening tool to assess the damage tolerance of turbine disk alloys.

APPENDIX A

STRESS INTENSITY CALCULATIONS FOR CORNER CRACK SPECIMEN

The stress intensity factor K_I at the specimen surface was calculated for the corner crack specimen by the following formulas (ref. 7):

$$K_I = 1.16 \left(\frac{2}{\pi}\right) \sigma \sqrt{\pi a} \quad \text{for} \quad a/w < 0.2$$

For higher values of a/w the following equation was used:

$$K_I = \left[1.12 - 0.13 \left(\frac{a}{w}\right) + 1.84 \left(\frac{a}{w}\right)^2 + 0.11 \left(\frac{a}{w}\right)^3 + 0.8 \left(\frac{a}{w}\right)^4\right] \left(\frac{2}{\pi}\right) \sigma \sqrt{\pi a}$$

where

a length of crack, m

σ nominal stress, MPa

w width of specimen, m

K_I stress intensity factor, MPa$\sqrt{m}$

APPENDIX B

CRACK LENGTH CALCULATION FOR COMPACT TENSION SPECIMEN

The crack length a of the compact tension specimen was calculated from the notch voltage V_n by using a normalized calibration curve. Hicks and Pickard (ref. 2) and Mom (ref. 7) reported such a normalized calibration curve (fig. 16) for a compact tension specimen. The normalized calibration curve, developed using finite element analysis, establishes a relationship between the crack parameter a/w and the voltage parameter V_n/V_{ref}. The relationship corresponding to the calibration curve can be mathematically expressed as follows (from ref. 7):

$$\frac{V_n}{V_0} = A + A_1\left(\frac{a}{w}\right) + A_2\left(\frac{a}{w}\right)^2 + A_3\left(\frac{a}{w}\right)^3 \qquad \text{(B1)}$$

where

V_n notch voltage

$V_0 = V_{ref}$ reference voltage

and

$A = 0.5766$

$A_1 = 1.9169$

$A_2 = -1.0712$

$A_3 = 1.6898$

Alternatively

$$\frac{a}{w} = B + B_1\left(\frac{V_n}{V_0}\right) + B_2\left(\frac{V_n}{V_0}\right)^2 + B_3\left(\frac{V_n}{V_0}\right)^3 \qquad \text{(B2)}$$

where

$B = -0.5051$

$B_1 = 0.8857$

$B_2 = -0.1398$

$B_3 = 2.398 \times 10^{-4}$

The final value (before the specimen was separated into two pieces under tensile loading) of the parameter V_n/V_{ref} was calculated from the measured values of V_n and V_{ref} for each specimen. The final value of the same parameter was also calculated from the normalized calibration curve (eq. (B1)) by using the measured average final crack length. In general, these two values

would not be the same, since at the beginning of the experiment it would be difficult to obtain a notch voltage that is identical to the reference voltage. Hence the following ratio was computed for each specimen:

$$NP = \frac{\left(\frac{V_n}{V_{ref}}\right)_{final,measured}}{\left(\frac{V_n}{V_{ref}}\right)_{final,normalized}}$$

where NP is the normalizing parameter.

The calibration was verified for each specimen in the following manner:

(1) The measured initial voltage ratio V_n/V_{ref} was normalized with the normalizing parameter NP.

$$\left(\frac{V_n}{V_{ref}}\right)_{initial,normalized} = \left(\frac{1}{NP}\right)\left(\frac{V_n}{V_{ref}}\right)_{initial,measured}$$

(2) The normalized initial voltage ratio was then used together with equation (B2) to calculate the initial crack length. This calculated initial crack length was compared with the measured initial crack length to verify the accuracy of the calibration.

At regular intervals of cyclic lives the measured voltage ratios were computed, and these ratios were normalized for each specimen with its normalizing parameter. The normalized voltage ratio was then used together with the normalized calibration curve (eq. (B2)) to compute the crack length a. The ASTM E647 standard (ref. 9) was used to truncate the initial crack propagation data.

REFERENCES

1. Wei, R.P.; and Brazill, R.L.: An Assessment of A-C and D-C Potential Systems for Monitoring Fatigue Crack Growth. Fatigue Crack Growth Measurement and Data Analysis, ASTM STP-738, S.J. Hudak, Jr., and R.J. Bucci, eds., ASTM, 1981, pp. 103-119.

2. Hicks, M.A.; and Pickard, A.C.: A Comparison of Theoretical and Experimental Methods of Calibrating the Electrical Potential Drop Technique for Crack Length Determination. Int. J. Fract., vol. 20, no. 2, 1982, pp. 91-101.

3. Gangloff, R.P.: Electrical Potential Monitoring of Fatigue Crack Formation and Growth From Small Defects. General Electric, Report No. 79CRD267, Jan. 1980, pp. 1-21.

4. Van Stone, R.H.; Krueger, D.D.; and Duvelius, L.T.: Use of a d-c Potential Drop Crack Monitoring Technique in the Development of Defect Tolerant Disk Alloys. Fracture Mechanics: Fourteenth Symposium, Vol. 2, Testing and Applications, ASTM STP-791, J.C. Lewis and G. Sines, eds., ASTM, 1983, pp. II-553 to II-578.

5. Van Stone, R.H.; and Richardson, T.L.: Potential-Drop Monitoring of Cracks in Surface-Flawed Specimens. Automated Test Methods for Fracture and Fatigue Crack Growth, ASTM STP-877, W.H. Cullen, et al., eds., ASTM, 1985, pp. 148-166.

6. Mom, A.J.A.; and Raizenne, M.D.: AGARD Cooperative Programme on Titanium Alloy Engine Disc Material. Damage Tolerance Concepts for Critical Components, AGARD CP-393, 1985, pp. 9-1 to 9-9.

7. Mom, A.J.A.: Working Document for the AGARD Cooperative Test Programme on Titanium Alloy Engine Disc Material. National Aerospace Laboratory, The Netherlands, NLR TR 84022 L, 1984.

8. Mom, A.J.A.; and Raizenne, M.D.: AGARD Engine Disc Cooperative Test Programme - Core Programme Results. National Aerospace Laboratory, The Netherlands, NLR MP 86045 U, 1987.

9. Standard Test Method for Constant-Load-Amplitude Fatigue Crack Growth Rates Above 10^{-8} m/Cycle. E647-86, Metals Test Methods and Analytical Procedures, Annual Book of ASTM Standards, Section 3, Vol. 03.01, ASTM, 1986, pp. 714-736.

10. Hartman, G.A.; and Johnson, D.A.: DC Electric-Potential Method Applied to Thermal/Mechanical Fatigue Crack Growth. Experimental Mechanics, vol. 27, no. 1, Mar. 1987, pp. 106-112.

11. Bachmann, V.; and Munz, D.: Fatigue Crack Closure Evaluation With the Potential Method. Eng. Fract. Mech., vol. 11, no. 1, 1979, pp. 61-71.

12. Pearson, S.: Initiation of Fatigue Cracks in Commercial Aluminum Alloys and the Subsequent Propagation of Very Short Cracks. Eng. Fract. Mech., vol. 7, no. 2, 1975, pp. 235-247.

13. Morris, W.L.; Buck, O.; and Marcus, H.L.: Fatigue Crack Initiation and Early Propagation in AL 2219-T851. Metall. Trans., A., vol. 7, no. 8, Aug. 1976, pp. 1161-1165.

14. Telesman, J.; Fisher, D.M.; and Holka, D.: Variables Controlling Fatigue Crack Growth of Short Cracks. Fatigue Life: Analysis and Prediction, V.S. Goel, ed., American Society for Metals, 1986, pp. 53-67.

TABLE I. - MINIMUM MEASURED ROOM-TEMPERATURE

MATERIAL PROPERTIES OF Ti-6Al-4V ALLOY DISK

[From ref. 8.]

Tensile strength, MPa	969
0.2-Percent yield strength, MPa	865
Reduction in area, percent	26
Fracture toughness, MPa$\sqrt{m}$	52.3

TABLE II. - TEST MATRIX OF Ti-6Al-4V FCG PROGRAM

Type of test		LCF life/crack initiation		Crack propagation	
Test specimen		Smooth cylindrical	Double-edge-notched ($K_t \sim 2.2$)	Corner crack	ASTM compact tension
Number of specimens		6	6	3	3
Crack detection	EPDT		✓	✓	✓
	Optical			✓	
	Goal	Baseline fatigue life data	Only initial crack formation	"Short" crack range	Total da/dN-ΔK curve

TABLE III. - Ti-6Al-4V LOW-CYCLE-FATIGUE DATA

[R = 0.1.]

Specimen	Stress range, $\Delta\sigma = \sigma_{max} - \sigma_{min}$, MPa	Number of cycles to failure, N_f
LCF 9	809.2	2 679
LCF 8	808.6	2 350
LCF 7	778.9	5 510
LCF 12	765.9	11 016
LCF 10[a]	750.6	8 156
LCF 11[b]	746.7	11 327

[a]Specimen failed outside the gage section.
[b]Specimen failed near one of the knife edges of the extensometer.

TABLE IV. - Ti-6Al-4V FATIGUE CRACK INITIATION DATA

FOR DOUBLE-EDGE-NOTCHED SPECIMENS

[K_t = 2.2; R = 0.1.]

Specimen	Stress range, $\Delta\sigma = \sigma_{max} - \sigma_{min}$, MPa	Number of cycles to crack initiation, $N_{1\%}$	Number of cycles to failure, N_f
K_t 12	775	2 575	2 890
K_t 9	775	4 050	4 340
K_t 8	625	8 950	9 810
K_t 7	625	9 200	9 660
K_t 10	500	25 100	27 120
K_t 11	500	27 000	29 350

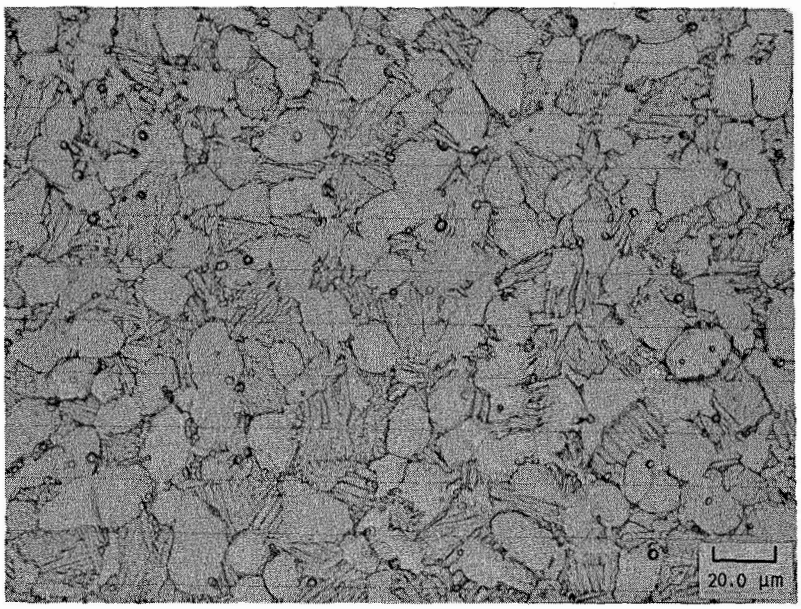

FIGURE 1. - MICROSTRUCTURE OF Ti-6Al-4V ALLOY USED IN THIS STUDY.

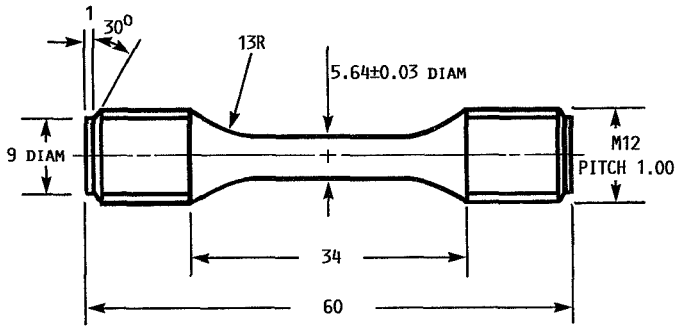

(a) CYLINDRICAL UNNOTCHED LCF SPECIMEN. REFERENCE CROSS SECTION, 25 mm^2.

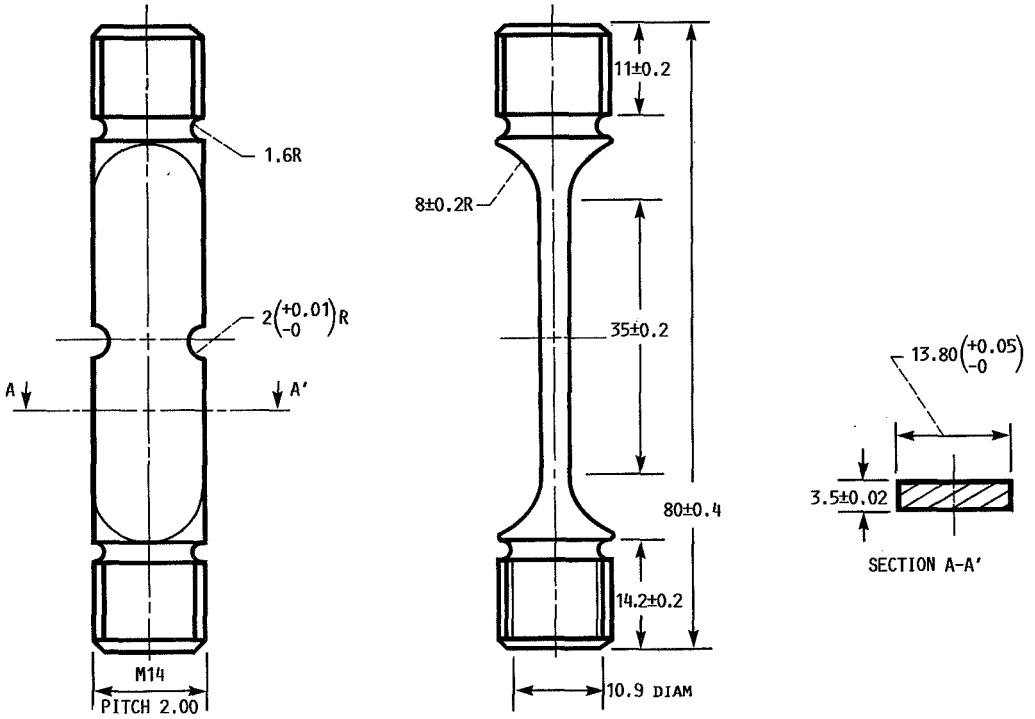

(b) FLAT DOUBLE-EDGE-NOTCHED SPECIMEN (NOMINAL STRESS CONCENTRATION FACTOR, $K_t \sim 2.2$).

FIGURE 2. - TEST SPECIMENS. (LINEAR DIMENSIONS ARE IN MILLIMETERS.)

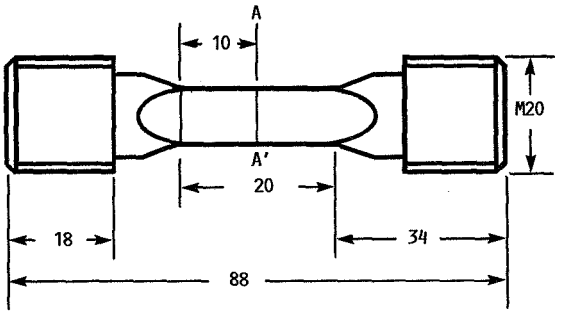

(c) CORNER CRACK SPECIMEN. NOTCH DEPTH, 0.25 MM; NOTCH WIDTH, 0.10 MM.

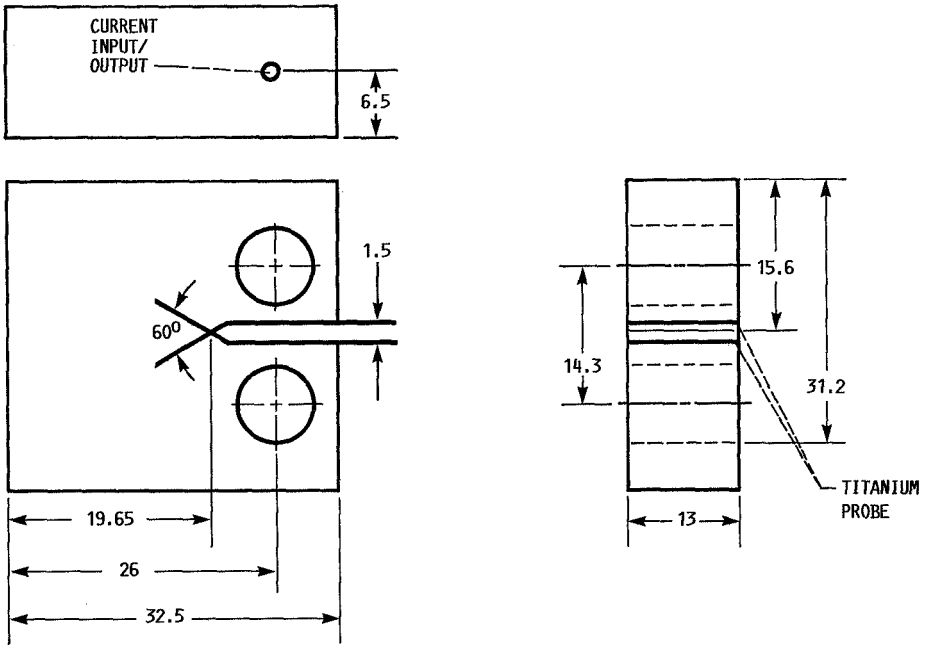

(d) COMPACT TENSION SPECIMEN.

FIGURE 2. - CONCLUDED.

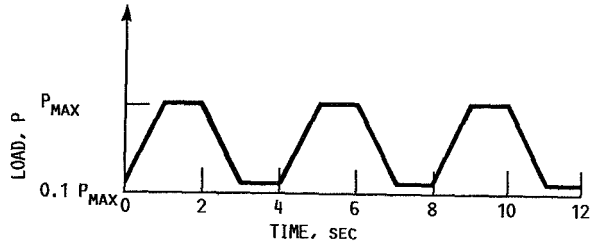

FIGURE 3. - SCHEMATIC ILLUSTRATION OF LOAD WAVE-FORM. $R = P_{MIN}/P_{MAX} = 0.1$.

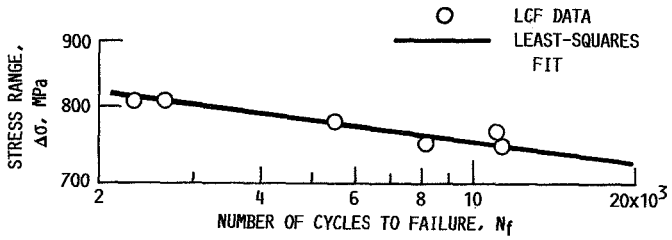

FIGURE 4. - RESULTS OF LCF EXPERIMENTS.

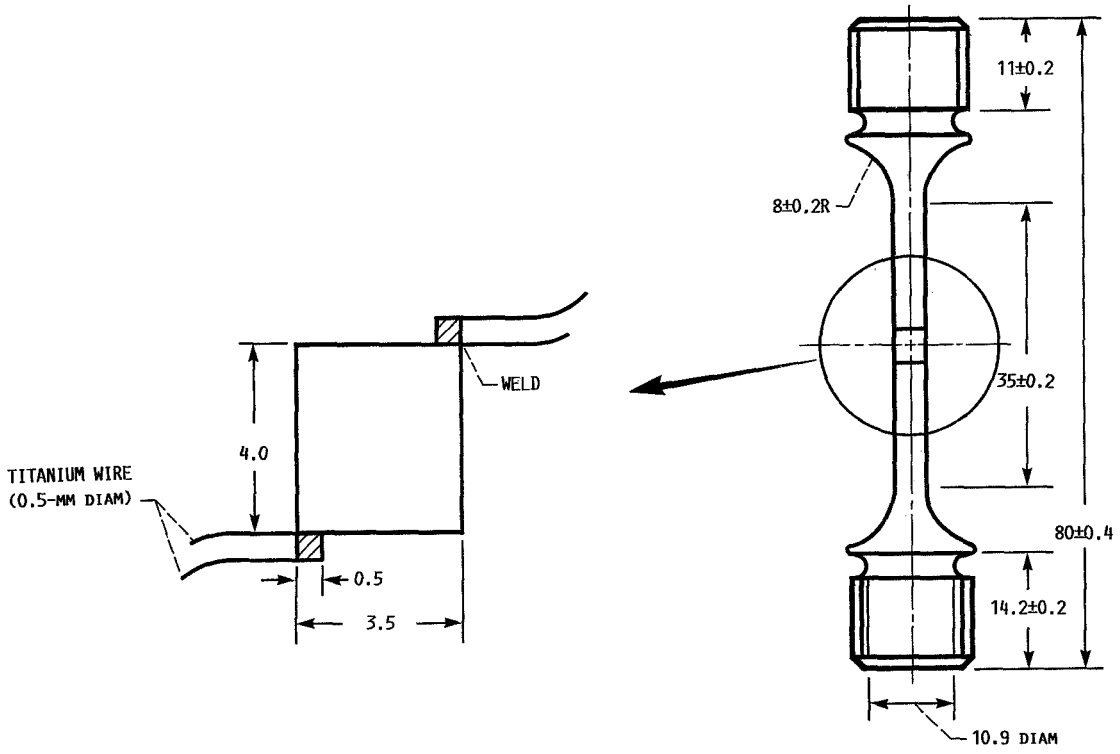

(a) ATTACHMENT OF POTENTIAL LEADS.

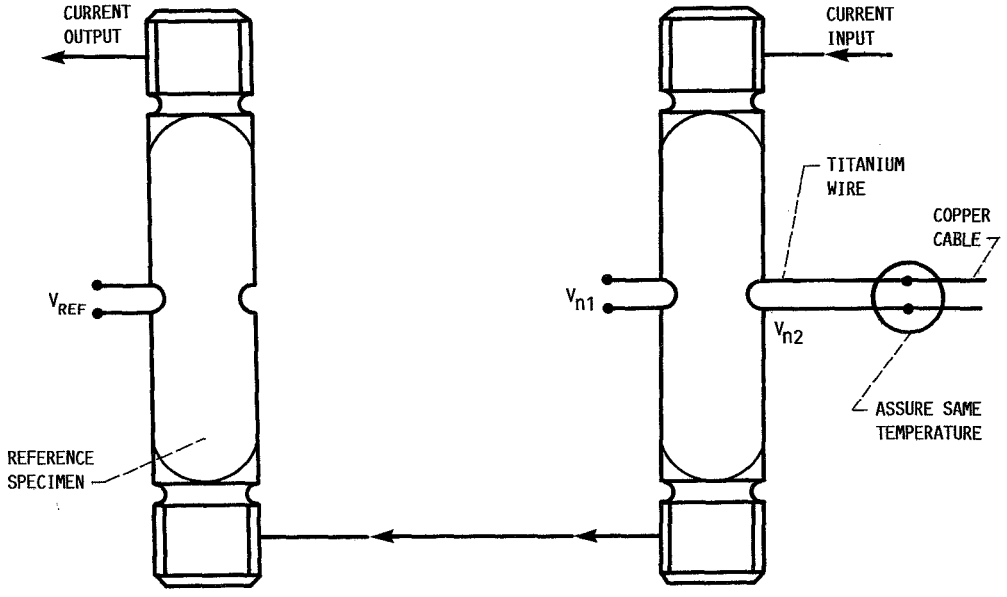

(b) SETUP OF CURRENT AND VOLTAGE WIRING.

FIGURE 5. - WIRING OF DOUBLE-EDGE-NOTCHED SPECIMENS. (ALL DIMENSIONS ARE IN MILLIMETERS.)

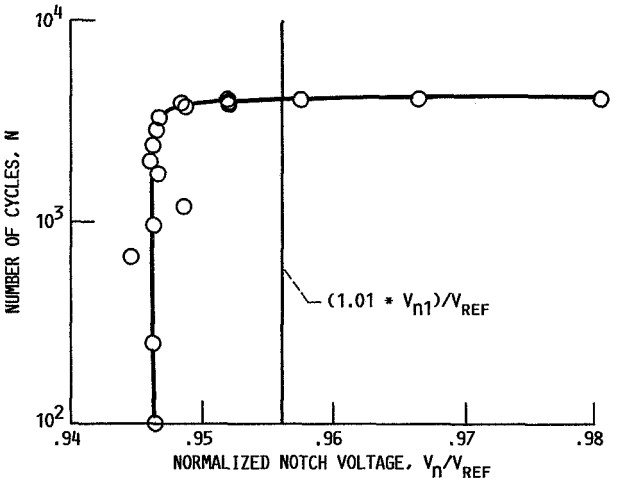

FIGURE 6. - NORMALIZED NOTCH VOLTAGE VERSUS NUMBER OF CYCLES FOR DOUBLE-EDGE-NOTCHED SPECIMEN. SPECIMEN NUMBER, K_t 9; CRACK INITIATION, $N_{1\%}$ = 4050; N_f = 4340.

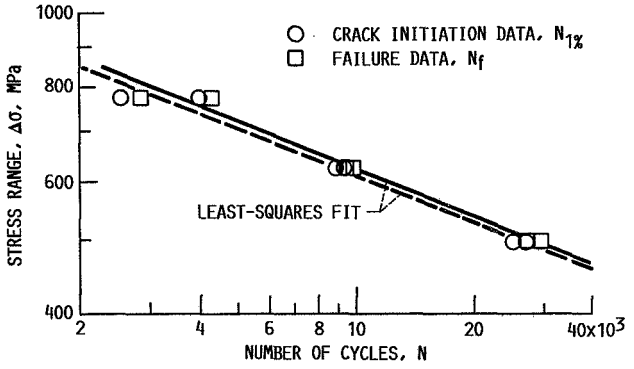

FIGURE 7. - RESULTS OF CRACK INITIATION EXPERIMENTS ON DOUBLE-EDGE-NOTCHED SPECIMENS.

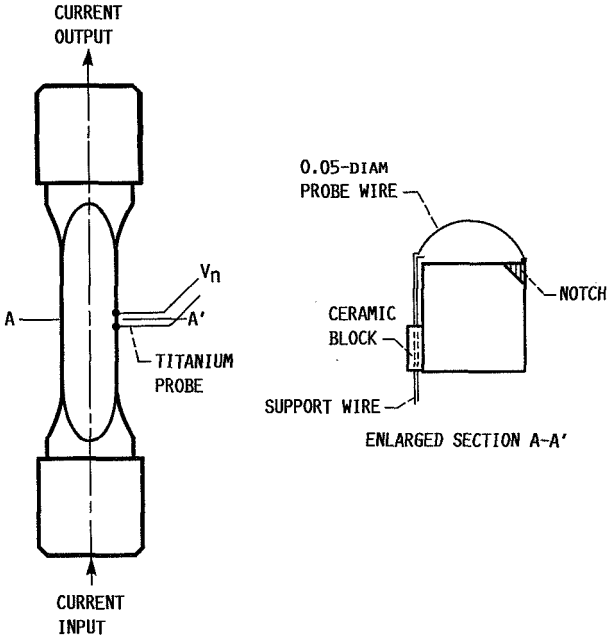

FIGURE 8. - POTENTIAL DROP LEAD LOCATIONS FOR CORNER CRACK SPECIMEN. (ALL DIMENSIONS ARE IN MILLIMETERS.)

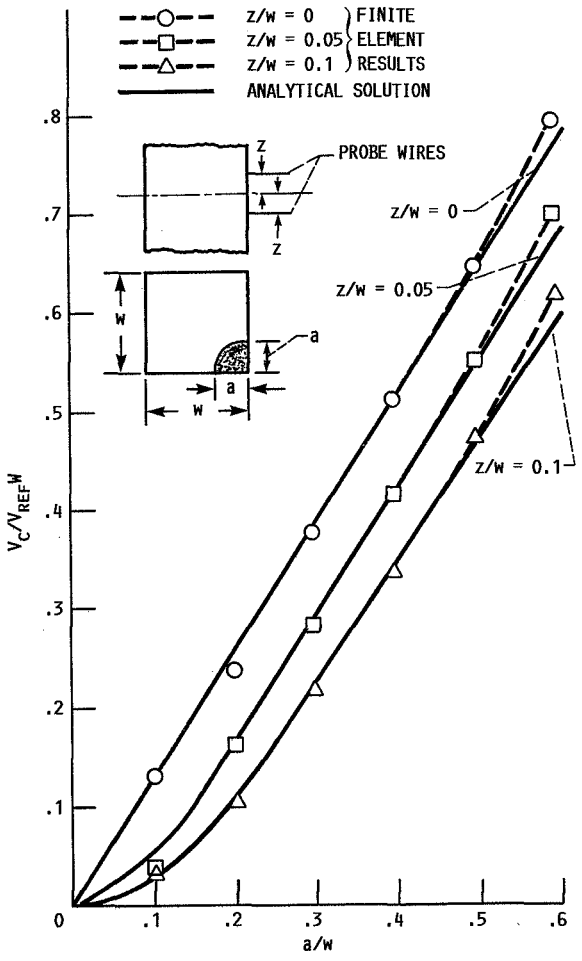

FIGURE 9. - COMPARISON OF ANALYTIC AND FINITE ELEMENT RESULTS FOR CORNER CRACK SPECIMEN. (FROM REF. 7.)

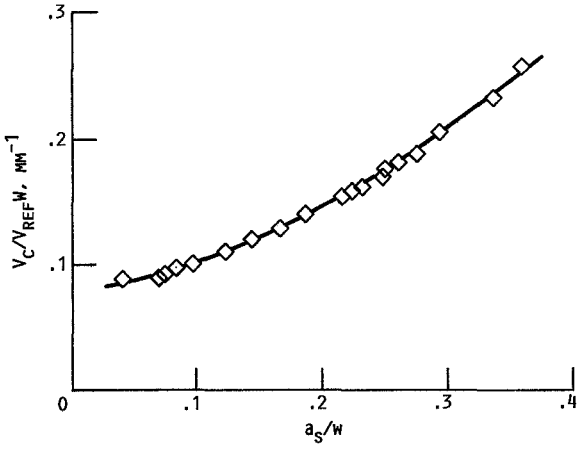

FIGURE 10. - MASTER CALIBRATION CURVE FOR CORNER CRACK SPECIMEN. z/w = 0.102.

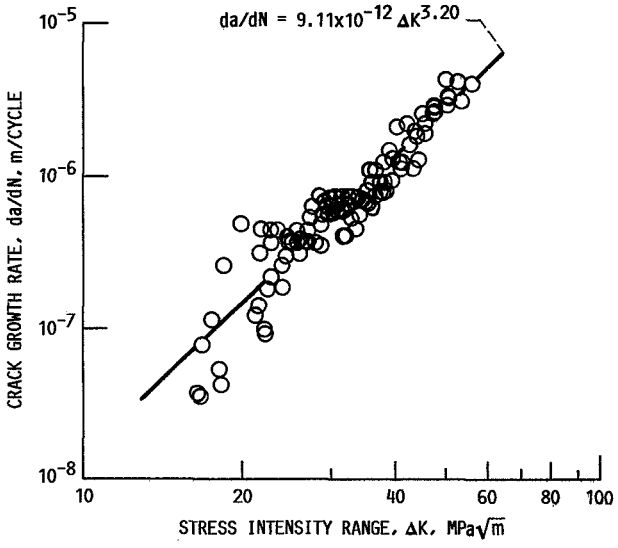

FIGURE 11. - FATIGUE CRACK GROWTH DATA OBTAINED WITH CORNER CRACK SPECIMENS.

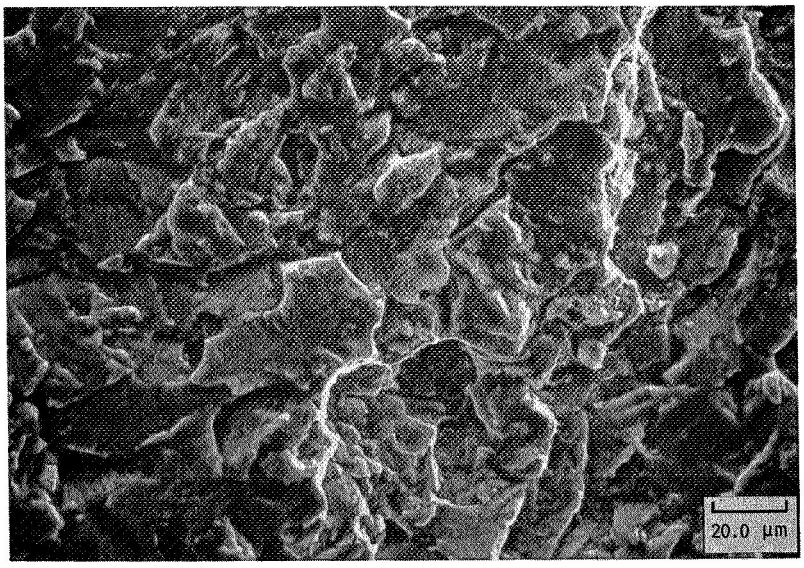

(a) CRYSTALLOGRAPHIC FRACTURE IN LOW ΔK REGIME.

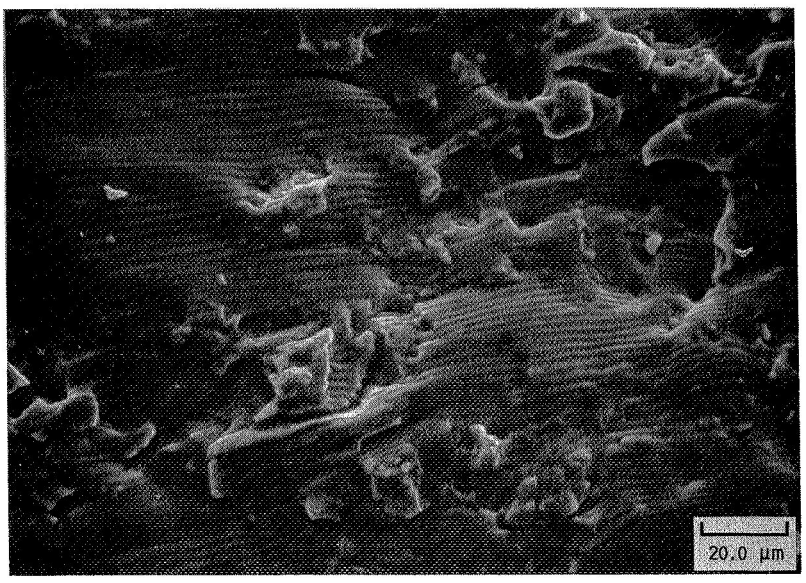

(b) STRIATION FORMATION IN INTERMEDIATE ΔK REGIME.

FIGURE 12. - REPRESENTATIVE FRACTOGRAPHS OF A CORNER CRACK SPECIMEN AT EARLY AND INTERMEDIATE STAGES OF FATIGUE CRACK GROWTH.

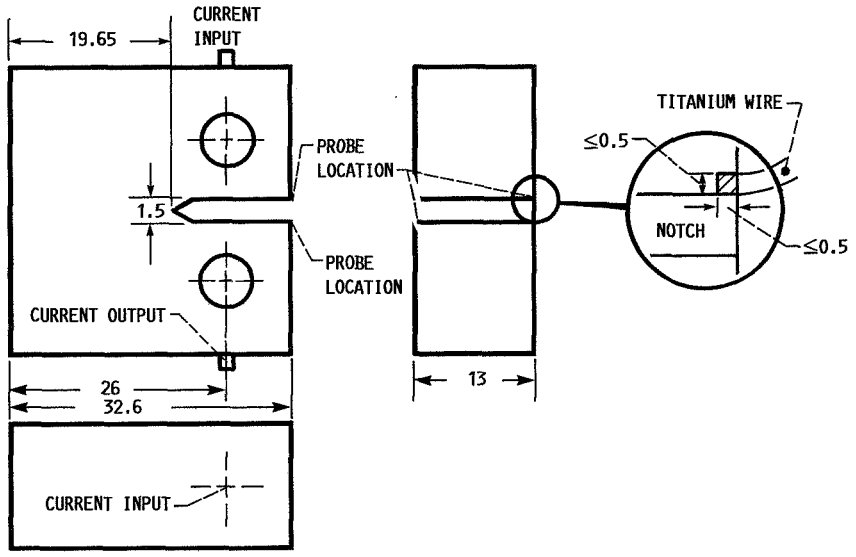

(a) ATTACHMENT OF CURRENT LEADS AND POTENTIAL PROBES.

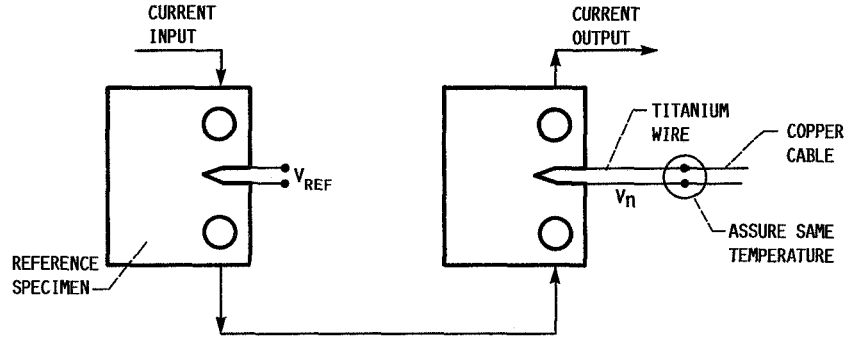

(b) SETUP OF CURRENT AND VOLTAGE WIRING. ($V_{REF,INITIAL} \approx V_{n,INITIAL}$.)

FIGURE 13. - WIRING OF COMPACT TENSION SPECIMENS. (ALL DIMENSIONS ARE IN MILLIMETERS.)

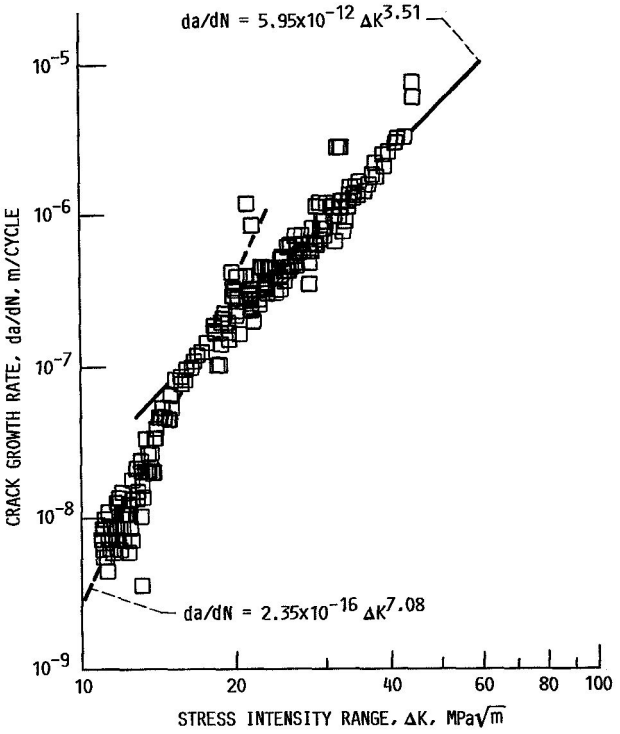

FIGURE 14. - FATIGUE CRACK GROWTH DATA OBTAINED WITH COMPACT TENSION SPECIMENS.

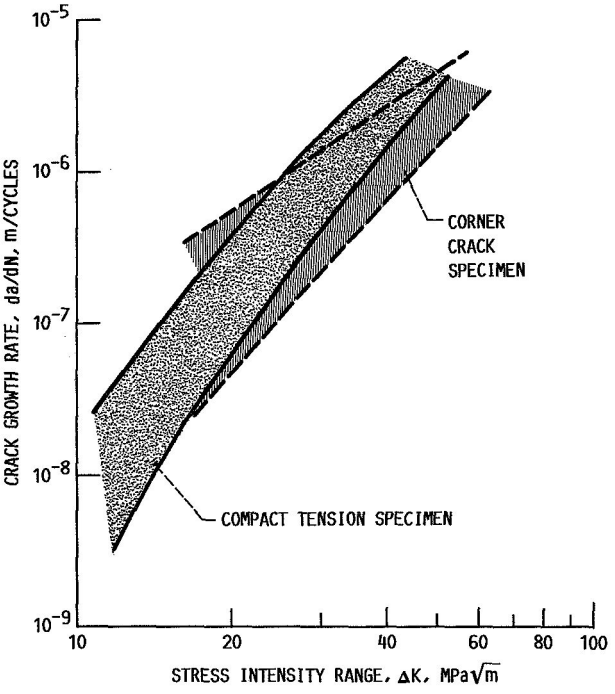

FIGURE 15. - COMPARISON OF FATIGUE CRACK GROWTH RATES FOR CORNER CRACK AND COMPACT TENSION SPECIMENS.

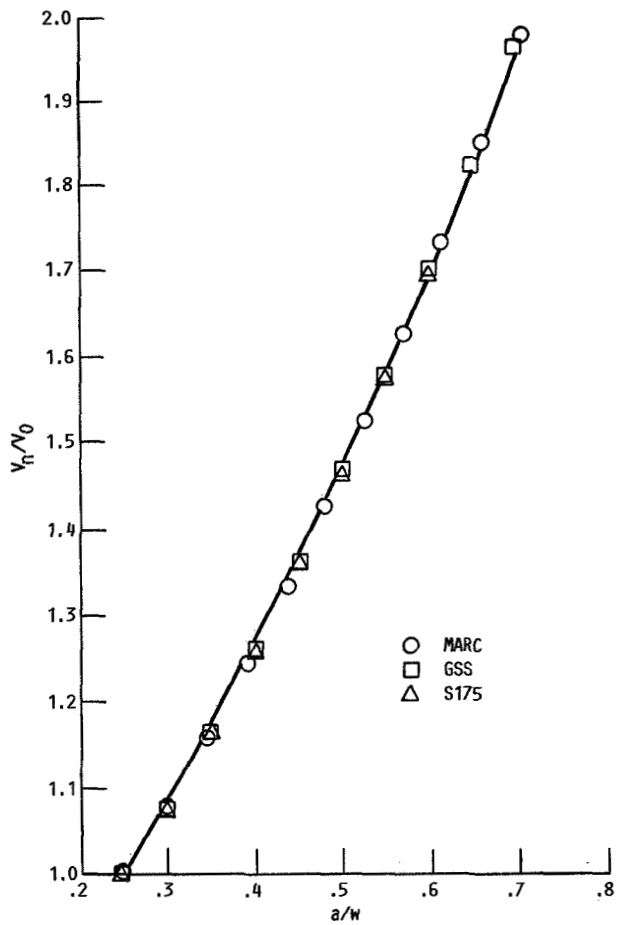

FIGURE 16. - FINITE ELEMENT POTENTIAL DROP ANALYSIS FOR COMPACT TENSION SPECIMEN NORMALIZED TO $V_n/V_0 = 1$ AT $a/w = 0.244$, WHERE V_0 IS POTENTIAL DROP AT INITIAL CRACK LENGTH a_0 AND V_n IS POTENTIAL DROP AT CRACK LENGTH a. (FROM REFS. 2 AND 7.)

NASA
National Aeronautics and Space Administration

Report Documentation Page

1. Report No.	2. Government Accession No.	3. Recipient's Catalog No.
NASA TM-100877		

4. Title and Subtitle

Characterization of Fatigue Crack Initiation and Propagation in Ti-6Al-4V With Electrical Potential Drop Technique

5. Report Date
July 1988

6. Performing Organization Code

7. Author(s)
Sreeramesh Kalluri and Jack Telesman

8. Performing Organization Report No.
E-4111

10. Work Unit No.
505-63-1B

9. Performing Organization Name and Address
National Aeronautics and Space Administration
Lewis Research Center
Cleveland, Ohio 44135-3191

11. Contract or Grant No.

13. Type of Report and Period Covered
Technical Memorandum

12. Sponsoring Agency Name and Address
National Aeronautics and Space Administration
Washington, D.C. 20546-0001

14. Sponsoring Agency Code

15. Supplementary Notes
Sreeramesh Kalluri, Sverdrup Technology, Inc., NASA Lewis Research Center Group, Cleveland, Ohio 44135; Jack Telesman, NASA Lewis Research Center.

16. Abstract

Electrical potential methods have been used in the past primarily to monitor crack length in long-crack specimens subjected to fatigue loading. In this study an attempt was made to develop test procedures for monitoring the fatigue crack initiation and the growth of short fatigue cracks in a turbine disk alloy with the electrical potential drop technique (EPDT). In addition, the EPDT was also applied to monitor the fatigue crack growth in long-crack specimens of the same alloy. The experimental program was conducted as part of an AGARD-sponsored roundrobin program on titanium alloy engine disk material. The resolution of the EPDT for different specimen geometries was determined. Factors influencing the EPDT are identified and the applicability of EPDT in implementing damage-tolerant design concepts for turbine disk materials is discussed. The experimental procedure adopted and the results obtained are presented. No substantial differences were observed between the fatigue crack growth data of short- and long-crack specimens.

17. Key Words (Suggested by Author(s))	18. Distribution Statement
Electrical potential drop technique; Fatigue; Crack initiation; Crack propagation; Damage tolerance	Unclassified - Unlimited Subject Category 39

19. Security Classif. (of this report)	20. Security Classif. (of this page)	21. No of pages	22. Price*
Unclassified	Unclassified	24	A02

NASA FORM 1626 OCT 86

*For sale by the National Technical Information Service, Springfield, Virginia 22161

National Aeronautics and
Space Administration

Lewis Research Center
Cleveland, Ohio 44135

SECOND CLASS MAIL

ADDRESS CORRECTION REQUESTED

Official Business
Penalty for Private Use $300

Postage and Fees Paid
National Aeronautics and
Space Administration
NASA-451